Journal of Southeast University (English Edition) Vol. 36, No. 4, pp. 475 - 482 Dec. 2020 ISSN 1003—7985

Mechanism of coconut husk activated carbon modified by $Mn(NO_3)_2$

Huang Bangfu Shi Zhe Cai Ming Yu Anhe

(Faculty of Metallurgical and Energy Engineering, Kunming University of Science and Technology, Kunming 650093, China)
(Clean Metallurgy Key Laboratory of Complex Iron Resources of the University in Yunnan Province, Kunming University of Science and Technology, Kunming 650093, China)

Abstract: To study the mechanism by which activated carbon is modified by HNO_3 and $Mn(NO_3)_2$, the pore texture and surface chemical characteristics of carbon materials in coconut husk activated carbon (AC) were examined via scanning electron microscopy (SEM), Brunauer-Emmett-Teller (BET), X-ray diffraction (XRD), Fourier-transform infrared spectroscopy (FTIR), and X-ray photoelectron spectroscopy (XPS). After being modified by HNO_3, the millipore character of AC became deformed, and the character of the adjacent pores remained consolidated. The surface manganites of Mn/AC-1 presented as block and reticular fiber structures, Mn/AC-2's surface manganites presented as petty mammock crystals, and Mn/AC-3's surface manganites were observed as gauze nanosheets that interlace to fill in the pore canal. Nitric acid modification was shown to enlarge surface pores but decrease the specific surface area of AC. Mn loading can be used to construct a new pore structure that, in turn, increased the total specific surface area as well as the specific surface area and the volume of the millipores. Mn/AC-2's pore structure was optimized at a calcination temperature of 500 ℃ and a loading quantity of 5%. The ash content of AC was considerably reduced after modified by HNO_3. The active materials for Mn/AC-1 mainly consisted of Mn_3O_4, with a few Mn_2O_3 crystals, whereas Mn/AC-2's materials were mainly Mn_3O_4 and some MnO crystals. Mn/AC-3 was exclusively composed of Mn_3O_4. HNO_3 activation and Mn loading modification did not considerably affect the functional group species present on the catalyst. Modification conditions using the same loading quantities and higher calcination temperatures decreased the number of O—H and N—H bonds while conversely increasing the number of C═C and C—O bonds. On the contrary, the use of a higher loading quantity while maintaining the same calcination temperature increased the number of O—H and N—H bonds. A higher loading quantity is beneficial for increasing Mn^{4+} species. A higher calcination temperature is beneficial for increasing Mn^{3+} species. The results can optimize the conditions under which Mn/AC catalyst modification occurs, thus improving the physical and chemical properties of carbon-based sorbents.

Key words: HNO_3; $Mn(NO_3)_2$; coconut husk activated carbon; physicochemical property; modification mechanism

DOI: 10.3969/j.issn.1003-7985.2020.04.013

Received 2020-05-15, **Revised** 2020-08-26.

Biography: Huang Bangfu (1983—), male, doctor, associate professor, kmusthbf@163.com.

Foundation items: The Science and Technology Plan of Yunnan Science and Technology Department (No. 2019FB077, 202001AT070029), the Open Fund of Key Laboratory of Ministry of Education for Metallurgical Emission Reduction and Comprehensive Utilization of Resources (No. JKF19-08), the Industrialization Cultivation Project of Scientific Research Fund of Yunnan Provincial Department of Education (No. 2016CYH07).

Citation: Huang Bangfu, Shi Zhe, Cai Ming, et al. Mechanism of coconut husk activated carbon modified by $Mn(NO_3)_2$ [J]. Journal of Southeast University (English Edition), 2020, 36(4): 475 - 482. DOI: 10.3969/j.issn.1003-7985.2020.04.013.

Actived carbon (AC) is a good catalytic carrier and is sorbent due to its large specific surface area and the presence of numerous surface functional groups as well as its chemical stability and favorable adsorptive properties. AC is often used in sewage treatment and gas cleaning applications because it is an abundant material that is commonly available from stable sources[1-3]. The acidity, adsorption capacity, and catalytic performance of coconut husk AC are all determined by its pore structure and the quantity of associated surface functional groups. Thus, the physicochemical properties of AC form the foundation for the adsorption of polar and nonpolar materials. Unmodified coconut husk AC has been shown to exhibit limited adsorptive properties compared with modified coconut husk AC.

Previous studies[4-8] have shown that AC modified by MnO_x, CuO, Fe_2O_3, and CeO_2 exhibited low-temperature catalytic activity. In particular, the active metal oxide, MnO_x, has an amorphous valence state and high acidic strength and is renowned for the ease with which voltinism occurs. Catalysts modified by the Mn species have a high oxygen content and are less prone to losing specific surface area and pore diameter[6-9]. The conditions under which modification occurs eventually determine the valence state and surface topography of a manganite on the catalyst under investigation. Existing research has mainly focused on the desulfurization and denitrification performance of carbon-based loaded Mn catalyst[10-12]. However, very few studies have carefully evaluated the mechanism by which Mn/AC is prepared using $Mn(NO_3)_2$.

To understand how $Mn(NO_3)_2$ affects AC, coconut husk AC modified using HNO_3 and $Mn(NO_3)_2$ was investigated. The effects of HNO_3 and $Mn(NO_3)_2$ on the pore texture and surface chemical characteristics of carbon materials were examined using scanning electron microscopy (SEM), Brunauer-Emmett-Teller (BET), X-ray diffraction (XRD), Fourier-transform infrared spectroscopy (FTIR), and X-ray photoelectron spectroscopy (XPS). The surface topography, pore structure, type of active material, and functional groups associated with AC, HNO_3/AC, and Mn/AC were systematically studied to optimize the conditions under which the modification of the Mn/AC catalyst occurs and to improve the physical and chemical properties of carbon-based sorbents.

1 Experimental

1.1 Catalyst preparation

Coconut husk AC (Chongqing Huaxi Cativated Create Factory) was used as the pure carbon material. The AC was washed with distilled water and soaked in a water bath for 2 h before being dried in an oven at 100 ℃. The AC sample was immersed in 4 mol/L of nitric acid at 80 ℃ for 2 h. The HNO_3/AC product was obtained by drying the sample in an oven at 100 ℃.

10 g of the HNO_3/AC sample were then immersed in $Mn(NO_3)_2$ liquor (100 mL) and ultrasonically stirred for 24 h. Afterward, the sample was dried at 102 ℃ for 4 h. Using a programmed rate of 15 ℃/min, the dried sample was calcined in a vacuum tube furnace for 3 h. The resulting Mn/AC catalyst subjected to the modification conditions is given in Tab. 1.

Tab. 1 Catalyst of Mn/AC preparation condition

Samples	m(Mn) : m(AC)/%	Calcination temperature/℃
Mn/AC-1	5	400
Mn/AC-2	5	500
Mn/AC-3	10	400

1.2 Material characterization

To study the changes in the samples' surface microtopography before and after modification, the microstructure of the carbon materials was investigated via SEM using a XL30 ESEM-TMP microscope. The BET surface areas of AC, HNO_3/AC, and Mn/AC were measured via an N_2 adsorption isotherm at 77 K using an UADRASORB-EVO analyzer. Total pore and micropore volumes were obtained using the Barret-Joyner-Halenda (BJH) method. Characteristics such as pore size distribution, pore volume, and the type of pore canal were obtained by analyzing the adsorption tendency of the catalyst. To confirm the phase composition of AC, HNO_3/AC, and Mn/AC, a PHI5000 VERSAPROBE-Ⅱ analyzer was used to conduct XRD experiments. FTIR spectra were recorded using a Fourier-transform infrared spectrometer (NICOLET IS10) to study changes in the surface functional groups of AC, HNO_3/AC, and Mn/AC. To obtain the information about the oxidation state of manganese on the catalyst surface and ensure the chemical compositions of the surface layer, XPS spectra of Mn/AC were recorded using a multifunctional scanning imaging photoelectron spectrometer (PHI5000 VERSAPROBE-Ⅱ).

2 Results and Discussion

2.1 SEM results

Surface microtopography (500 × magnification) of the samples before and after modification by HNO_3 is shown in Fig. 1(a) and Fig. 1(b). As shown in Fig. 1(a), coconut husk AC developed a clear pore structure, a distinct boundary, a smooth wall of holes, and a faviform surface structure, whereas Fig. 1(b) shows that the surface microtopography of HNO_3/AC becomes unsymmetrical and disordered since the same area has more ditches and air void structures. Similarly, a number of gully-like pores formed on the surface.

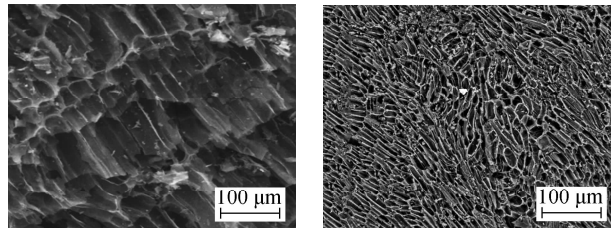

(a) (b)

Fig. 1 Scanning electron micrograph. (a) AC 500 ×; (b) HNO_3/AC 500 ×

The surface microtopography of Mn/AC-1 is shown in Fig. 2(a) and Fig. 2(b), whereas the surface microtopography of Mn/AC-2 is shown in Fig. 2(c) and Fig. 2(d). Details about the surface microtopography of Mn/AC-3 are given in Fig. 2(e) and Fig. 2(f). All images were taken at 2 000 × and 5 000 × magnification.

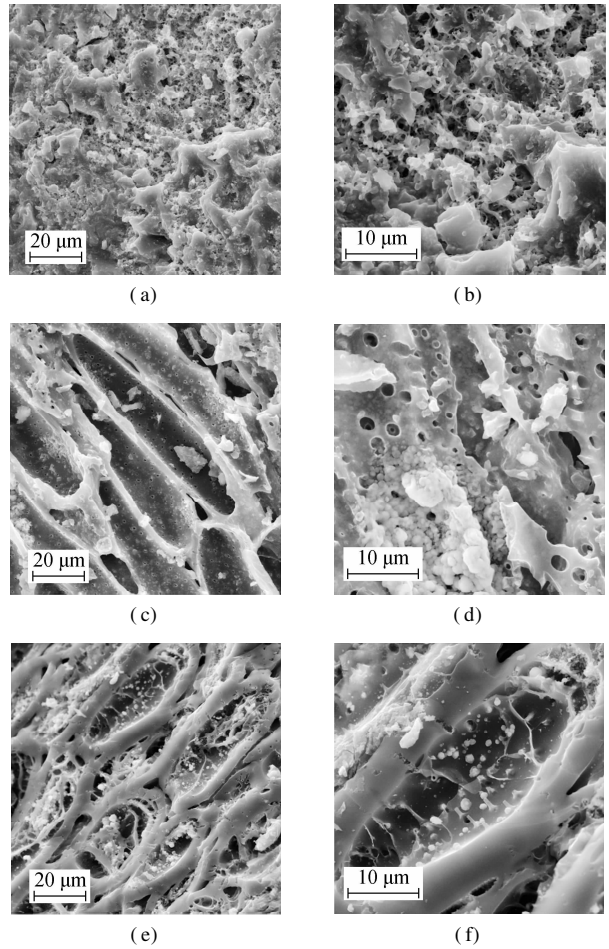

(a) (b)
(c) (d)
(e) (f)

Fig. 2 Scanning electron micrograph of Mn/AC. (a) Mn/AC-1 2 000 ×; (b) Mn/AC-1 5 000 ×; (c) Mn/AC-2 2 000 ×; (d) Mn/AC-2 5 000 ×; (e) Mn/AC-3 2 000 ×; (f) Mn/AC-3 5 000 ×

As shown in Figs. 2(a) and (b), manganites on the surface of Mn/AC-1 were present as block and network fiber structures. Block manganites were observed as laminiplantation that adhered to the surface of AC and almost completely covered the pore structures. However, the reticular fibers were observed as cross connections that maintained the adjacent pore space that had formed a multi-hole surface skeleton structure. New pore space structures supported more activated adsorption sites[13]. There were also network structures in the space between the blocks and on the surface of AC, which meant that the blocks had disappeared prior to their reformation as network fiber structures.

Figs. 2(c) and (d) show the disappearance of block and network fiber structures with increasing calcination temperatures. Petty mammock crystals were scattered across the surface of Mn/AC-2 with irregular shapes and an inset in the slit. Grainy manganites accumulated in the pore space structures and unveiled partly covered pore spaces. No large-scale blocking phenomenon was observed, and the pore space structures were clearly visible.

Compared with the phenomenon observed in Mn/AC-1, there was significantly improved distribution of the Mn/AC-3 manganites when the loading quantity was increased (see Figs. 2(e) and (f)). Large grains accumulated, and large voile-like nanosheets interlaced to fill the available pore space. Several uniform, compact nanosheets interlaced to form ordered network structures[14]. Grainy manganites adhered to the walls of the pore space that, in turn, exhibited prismatic perfection and net post structures.

2.2 BET results

The BET characterization results for the AC, HNO_3/AC, and Mn/AC catalysts are shown in Fig. 3, Fig. 4 and Tab. 2. As shown in Fig. 3(a), the volume of N_2 adsorbed by AC and HNO_3/AC rapidly increased during the initial stages at a low relative pressure due to the presence of numerous micropores. The numerous micropores that were present during the initial stages of N_2 adsorption on AC and HNO_3/AC can be defined as Type Ⅰ micropores according to the IUPAC classification scheme[15]. The diameters of the micropores were almost 2 nm, and the micropore structure that had developed occupied an immense specific surface area (see Tab. 2 and Fig. 3(b)). Calculations revealed that the micropore volume accounted for 69.97% of the total pore volume, and the micropore specific surface area accounted for 83.37% of the total specific surface area. This was the reason for the relative absence of mesopores and macropores. The average pore diameter and total pore volume increased slightly after nitric acid modification, and this was due to the opening of many previously closed pores, an action that was triggered by the reaction between nitric acid and carbon. This, in turn, caused some of the micropores to disappear and the

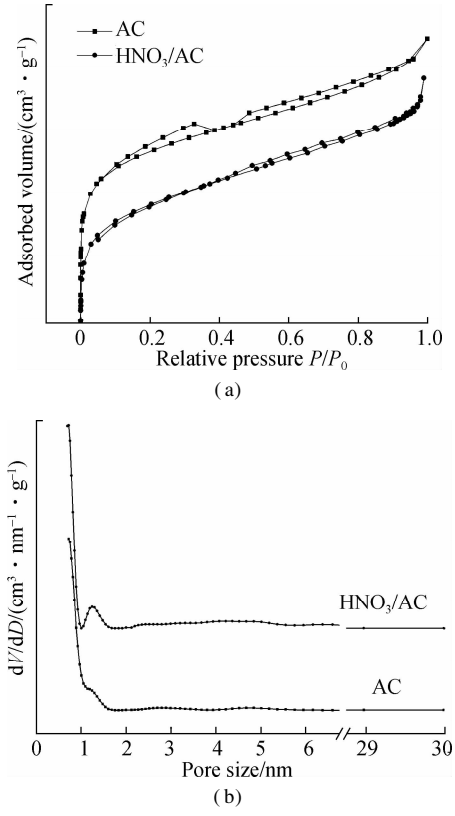

Fig. 3 AC and HNO_3/ACBET characterization. (a) Nitrogen isotherm adsorption-desorption curve; (b) Pore size distribution

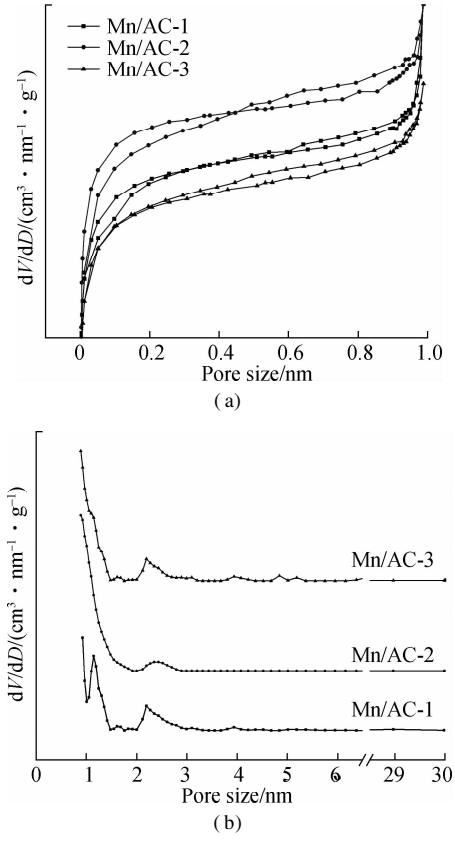

Fig. 4 Mn/ACBET characterization. (a) Nitrogen isotherm adsorption-desorption curve; (b) Pore size distribution

Tab. 2 Specific surface area and pore structure parameters of samples

Samples	S_{total}/($m^2 \cdot g^{-1}$)	S_{micro}/($m^2 \cdot g^{-1}$)	V_{total}/($cm^3 \cdot g^{-1}$)	V_{micro}/($cm^3 \cdot g^{-1}$)	D/nm
AC	786.690	655.840	0.383	0.268	2.301
HNO_3/AC	654.086	465.245	0.393	0.188	2.406
Mn/AC-1	733.855	653.407	0.361	0.257	2.046
Mn /AC-2	826.583	693.826	0.356	0.270	1.854
Mn /AC-3	720.463	616.857	0.321	0.243	1.912

carbon skeleton to collapse. Consequently, the micropore structure was destroyed; the micropore specific surface area decreased to 190.595 m^2/g; and the total specific surface area decreased to 132.604 m^2/g. Thus, although nitric acid modification enlarged the pores, it also resulted in a decrease in the specific surface area of AC.

The nitrogen isotherm adsorption-desorption curves and pore size distributions for Mn/AC are shown in Fig. 4. The numerous micropores that were present during the initial stages of N_2 adsorption on Mn/AC-1, Mn/AC-2, and Mn/AC-3 can also be defined as Type Ⅰ micropores according to the IUPAC classification scheme[15]. As shown in Fig. 4(b) and Tab. 2, the micropore contents are in the following order: Mn/AC-2 > Mn/AC-1 > Mn/AC-3. The volume of N_2 adsorbed on Mn/AC-1, Mn/AC-2, and Mn/AC-3 also rapidly increased under a high pressure. The reason for this may be that capillary condensation occurred under medium and high pressures in the relatively narrow free space. Thus, micropores and mesopores appeared as Type Ⅳ. A circular hysteresis ring was formed due to the condensation and evaporation processes within the capillaries that did not occur at the same pressure. The adsorption capacity of Mn/AC-2 was at its maximum, indicating the presence of narrower pore spaces and mesopores.

Compared with HNO_3/AC, the millipore volume, millipore specific surface area, and total specific surface area of Mn/AC-2 increased to 43.62%, 49.13%, and 26.37%, respectively. This tendency is also reflected in Mn/AC-1 and Mn/AC-3. The reason for this may be the block and network fiber of surface manganites, which formed new structures and increased the specific surface area. Compared with AC, Mn/AC-2 was shown to have optimized pore structure parameters. Thus, its total pore volume and diameter were lower than those of Mn/AC-1. The reason for this may have been the presence of grain manganites in the narrow slit and pore spaces that promoted the formation of more millipore structures. This, in turn, increased the specific surface area and decreased the pore diameter of Mn/AC-2. The pore structure parameters for Mn/AC-3 were the same as those for Mn/AC-1 and were shown to be inferior to the parameters for Mn/AC-2. The reason for this may be excess loading, which blocked the pore spaces and decreased the pore structure parameters.

2.3 XRD results

To analyze the change in the graphite crystal and Mn phase composition, XRD spectra for the AC, HNO_3/AC, and Mn/AC catalysts are obtained (see Fig. 5).

As shown in Fig. 5(a), a graphite peak was found in the XRD spectra for AC and HNO_3/AC in addition to two characteristic peaks of broad dispersion at 23.813° and 43.467° that corresponded to the 100 crystal face. Thus, it is clear that AC was composed of amorphous carbon. The diffraction peak observed at 23.813° was due to decompaction and tiering processes in the graphene layer at 2θ, whereas the diffraction peak at 43.467° was associated with the graphite crystal at 2θ. A diffraction peak that was linked to the 002 graphite crystal face at 2θ was observed at 26.468°[16]. From these results, it is clear that the diffraction peaks of the graphene layer and the graphite crystal became keen-edged due to a substantial reduction in the ash content of AC during the nitric acid

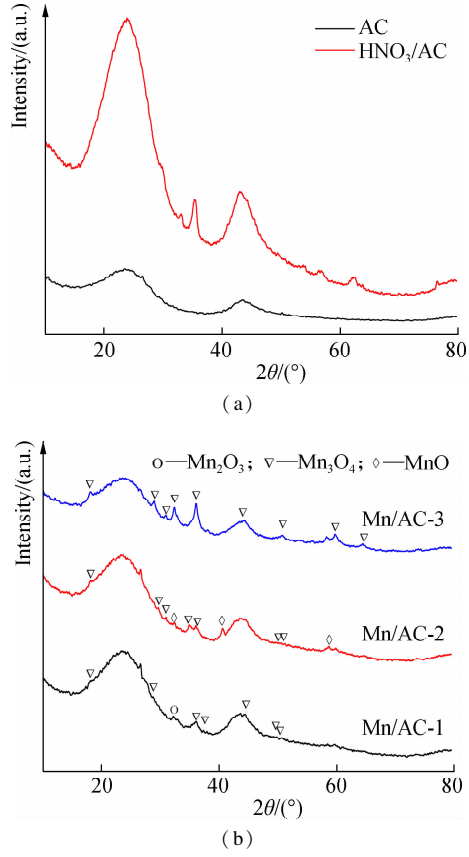

Fig. 5 XRD spectra for activated carbon before and after modification. (a) AC and HNO_3/AC; (b) Mn/AC

modification process.

According to JCPDS card No. 24-0734, diffraction peaks for Mn/AC-1 were observed at 18.013°, 28.833°, 36.085°, 37.952°, 44.466°, 49.832°, and 50.731°, which corresponded to the 101, 112, 211, 004, 220, 204, and 105 crystal faces of Mn_3O_4, respectively (see Fig. 5(b))[17]. The diffraction peak for Mn_2O_3 was noted at 32.966° and corresponded to the 222 crystal face of Mn_2O_3. The above studies show that when the loading quantity was 5% and the calcination temperature was 400 ℃, the manganites observed were mainly composed of Mn_3O_4, with few Mn_2O_3 crystals.

However, when a higher calcination temperature was used with the same loading quantity, the diffraction peaks for Mn/AC-2 were shown at 17.998°, 28.919°, 30.972°, 36.031°, 36.368°, 44.437°, and 50.683°, all of which corresponded to the 101, 112, 200, 211, 202, 220, and 105 crystal faces of Mn_3O_4, respectively. According to JCPDS card No. 75-0626, the diffraction peaks at 34.899°, 40.578°, and 58.774° were assigned to the 111, 200, and 220 crystal faces of MnO, respectively[18]. The above studies show that when the calcination temperature was 500 ℃ and the loading quantity remained at 5%, the manganites observed in the reaction were mainly composed of Mn_3O_4 and only a few MnO crystals. This may be due to the deoxidization of the manganites via AC, which in turn resulted in the transition of Mn to a lower valence.

When the conditions were adjusted so that the calcination temperature remained the same while a higher loading quantity was used, i.e., the formation of Mn/AC-3, the diffraction peaks were observed at 18.034°, 28.934°, 30.998°, 32.357°, 36.073°, 44.457°, 50.701°, 59.828°, and 64.609° corresponding to the 101, 112, 200, 103, 211, 220, 105, 224, and 400 crystal faces of Mn_3O_4[19], respectively, without the presence of an interference peak. The above studies show that the manganites formed under these conditions were almost entirely composed of Mn_3O_4, resulting in keen-edged diffraction peaks and a higher degree of purity for the manganite crystals.

2.4 FTIR results

The adsorptive property of AC is influenced by its physical composition and chemical constitution. The quantity, type, and location of these functional groups are crucial to the chemical constitution of the catalyst. Generally, more functional groups tended to exist mainly on the micropore's surface, and few were found on the outside surface of activated carbon[20]. FTIR spectra for the AC, HNO_3/AC, and Mn/AC catalysts are shown in Fig. 6.

The FTIR spectra for AC are shown in Fig. 6(a). According to previous studies[21-22], the peak at 3 420 cm^{-1}

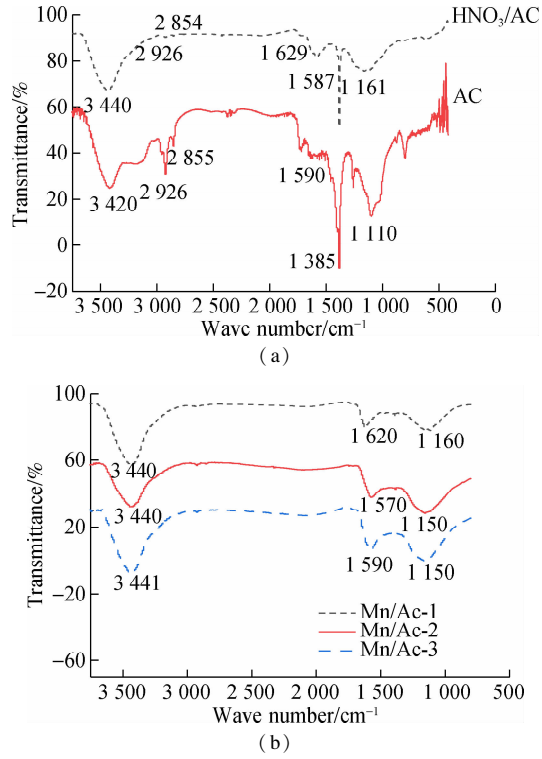

Fig. 6 FTIR spectra. (a) AC and HNO_3/AC; (b) Mn/AC-1, Mn/AC-2, and Mn/AC-3

was assigned to the phenolic O—H and the N—H bond of the amidocyanogen group, and the infrared luminosity of this peak was approximately 35%. The peaks observed at 2 926 and 28 55 cm^{-1} were associated with C—H antisymmetric and symmetry stretching vibrations that had an infrared luminosity of 29%. The peak at 1 590 cm^{-1} was assigned to C═C bond stretching vibrations, and the associated infrared luminosity was 24%. The peak at 1 385 cm^{-1} was assigned to the carbonyl group, and the infrared light luminosity of this peak was approximately 64%. The peaks at 1 110 cm^{-1} were assigned to the carboxylic acid anhydride and —OH bond vibrations[23-26], and the infrared luminosity of these peaks was 50%.

Compared with AC, the infrared luminosity of the peaks observed at 3 440 cm^{-1} was 26% for HNO_3/AC (see Fig. 6(a)), which diminished when the adsorption strength was increased. This was clear evidence that the number of O—H and N—H bonds within the structure had increased. The disappearance of the peaks at 2 926 and 2 854 cm^{-1} meant that almost no infrared light penetrated the HNO_3/AC structure; thus, the number of C—H bonds was comparatively greater than that in AC. The infrared luminosity of the peaks at 1 629, 1 587, and 1 388 cm^{-1} was less than that of AC, indicating that the number of C═C bonds and carbonyl groups within the structure had increased. Compared with AC's luminosity of 49%, the peak at 1 161 cm^{-1} had an infrared luminosity of 20%, which represented a decrease of more than half. This indicates that the number of carboxylic acid anhydride and —OH bond vibrations has increased by doub-

le. It can be inferred that CO and CO_2 were released after nitric acid oxidation, which in turn triggered ablation and pore structure deformation in AC. Oxygen-containing functional groups, such as carboxyls and esters, were formed after O and H had been adsorbed on the deformed pore structures[27] because the number of absorption active sites had increased. Fewer nitrogen-containing groups were generated on the surface.

The FTIR spectra for Mn/AC-1, Mn/AC-2, and Mn/AC-3 (see Fig. 6(b)) show the same tendencies as mentioned above. The infrared luminosity of the peaks observed at 3440 and 1620 cm^{-1} increased in varying degrees. This indicates that the number of bonds had decreased, that is, those that had been assigned as the phenolic O—H, the N—H bond of the amidocyanogen group, the C ═C bond, and the carbonyl group. The infrared luminosity of the peak observed at 1 160 cm^{-1} remained unchanged, indicating that the carboxylic acid anhydride and —OH bond vibrations were static. For Mn/AC-2, the infrared luminosity of the peak at 3 440 cm^{-1} was the same as that observed for HNO_3/AC. This supported the idea that the phenolic O—H and the N—H bonds of the amidocyanogen group were static. However, the infrared luminosity of the peaks observed at 1 570 and 1 150 cm^{-1} was shown to increase, and this was evidence of a decrease in the number of C ═C bonds, carbonyl groups, carboxylic acid anhydrides, and C—O bonds, all to varying degrees. For Mn/AC-3, the infrared luminosity values of the peaks at 3 441, 1 590, and 1 110 cm^{-1} were higher than those associated with HNO_3/AC. Again, this meant that the number of functional groups present had decreased, possibly because the functional groups were covered by manganites when a higher loading quantity was applied.

In summary, different Mn-loading conditions and HNO_3 activation methods did not affect the functional group species associated with the relevant catalyst. The functional group linked to HNO_3/AC decreased in varying degrees after Mn $(NO_3)_2$ loading modification processes were applied. The thorough distribution of the manganites meant that there was less blockage of the pore structures and less influence exerted on the associated functional groups.

2.5 XPS results

Previous studies[28] showed that the manganese species (Mn^{4+}, Mn^{3+}, Mn^{2+}, etc.) can be characterized by $Mn2p_{3/2}$ and $Mn2p_{1/2}$ peaks located between 639 and 658 eV. To confirm the relationship between the modified conditions and manganese species, the XPS spectra of Mn/AC were recorded. The characterization results are shown in Fig. 7.

As shown in Fig. 7(a), the Mn/AC-1 surface has 60.46% of Mn^{4+} species and 39.54% of Mn^{3+} species.

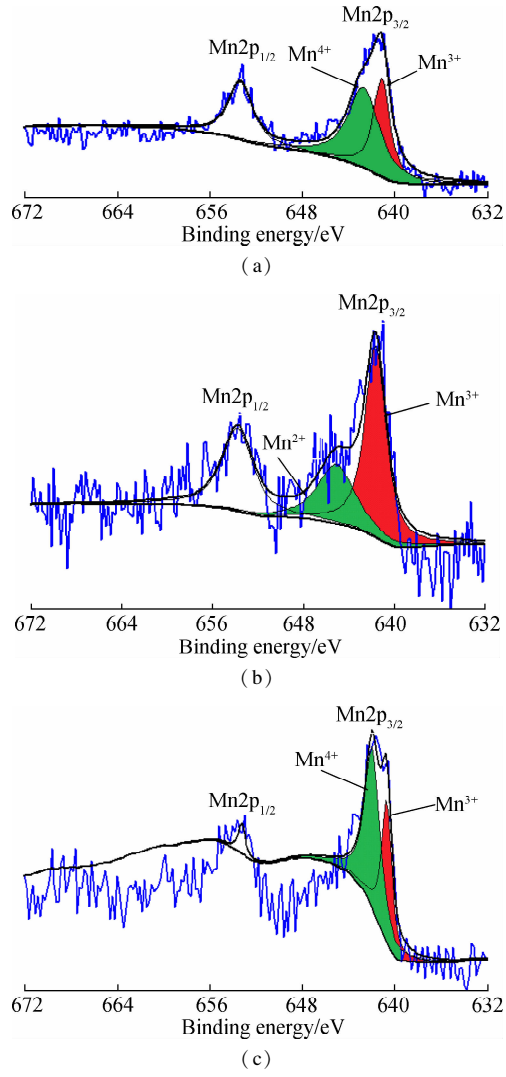

Fig. 7 XPS spectra of manganese species. (a) Mn/AC-1; (b) Mn/AC-2; (c) Mn/AC-3

In Fig. 7(b), with the same loading as Mn/AC-1, Mn/AC-2 prepared at a calcination temperature of 500 ℃ has 64.89% Mn^{3+} species and 35.11% Mn nitrate (Mn^{2+}); the Mn^{4+} species almost disappears. As shown in Fig. 7(c), at the same calcination temperature (400 ℃) as for Mn/AC-1, Mn/AC-3 prepared with 10% loading has 63.39% Mn^{4+} species, with the Mn^{3+} species reducing to 36.61%. In conclusion, a higher loading quantity is beneficial for increasing Mn^{4+} species, whereas a higher calcination temperature can increase Mn^{3+} species.

3 Conclusions

1) Coconut husk AC has a faviform surface structure in which the surface microtopography of HNO_3/AC becomes unsystematic and disordered. Manganites on Mn/AC-1 are present as block and network fiber structures in which the network fiber structures are preferentially formed at the expense of the blocks present in the system. Petty mammock crystals are scattered across the surface of Mn/AC-2, which experiences no large-scale blocking phenomenon and contains highly visible pore space struc-

tures. The manganites of Mn/AC-3 are well distributed, and they are composed of large voile-like nanosheets interlaced in a manner that fills in the available pore spaces. In this setting, the pore spaces represent prismatic perfection and net post structures.

2) Nitric acid modification enlarges the pores; however, this process decreases the specific surface area available. Compared with HNO_3/AC, Mn loading forms new pore structures and increases the total specific surface area available, millipore specific surface area, and millipore pore volume. Modification conditions under which the loading quantity is 5% and the calcination temperature is 500 ℃, result in more favorable numbers of pore structures on Mn/AC-2.

3) As AC is composed of amorphous carbon, its ash content is substantially reduced when it is modified with nitric acid. The manganites formed from Mn/AC-1 are mainly composed of Mn_3O_4 and a few Mn_2O_3 crystals. Mn/AC-2 manganites are mainly composed of Mn_3O_4 and some MnO crystals, and deoxidization of these manganites by AC results in a lower valence for Mn. Since the manganites of Mn/AC-3 are almost entirely made of Mn_3O_4, the diffraction peaks are keen-edged, and the degree of purity in the manganite crystals is higher.

4) Oxygen-containing functional groups are formed after O and H are adsorbed on pore structures that are deformed through the nitric acid modification process. A few nitrogen-containing groups are generated on the surface. The utilization of various Mn loading conditions and HNO_3 activation methods does not affect the functional group species under investigation. When the same loading quantity is employed at a higher calcination temperature, the number of O—H and N—H bonds decreases, whereas the number of C ═C and C—O bonds increases. Conversely, maintaining the same calcination temperature while using a higher loading quantity results in the formation of more O—H and N—H bonds.

5) The states of manganese on the Mn/AC catalyst surface are Mn^{4+}, Mn^{3+}, and Mn^{2+}. A higher loading quantity is beneficial for increasing Mn^{4+} species, whereas a higher calcination temperature can increase Mn^{3+} species.

References

[1] de Oliveira Ferreira M E, Vaz B G, Borba C E, et al. Modified activated carbon as a promising adsorbent for quinoline removal[J]. *Microporous and Mesoporous Materials*, 2019, **277**: 208 - 216. DOI: 10. 1016/j. micromeso. 2018. 10. 034.

[2] Nieto-Delgado C, Gutiérrez-Martínez J, Rangel-Méndez J R. Modified activated carbon with interconnected fibrils of iron-oxyhydroxides using Mn^{2+} as morphology regulator, for a superior arsenic removal from water[J]. *Journal of Environmental Sciences*, 2019, **76**: 403 - 414. DOI: 10. 1016/j. jes. 2018. 06. 002.

[3] Cao Y H, Wang K L, Wang X M, et al. Adsorption of butanol vapor on active carbons with nitric acid hydrothermalmodification [J]. *Bioresource Technology*, 2015, **196**: 525 - 532. DOI: 10. 1016/j. biortech. 2015. 08. 027.

[4] Yin S L, Zhu B Z, Sun Y L, et al. Effect of Mn addition on the low-temperature NH_3-selective catalytic reduction of NO_x over Fe_2O_3/activated coke catalysts: Experiment and mechanism[J]. *Asia-Pacific Journal of Chemical Engineering*, 2018, **13**(5): e2231. DOI: 10. 1002/apj. 2231.

[5] Qin Y H, Huang L, Zheng J X, et al. Low-temperature selective catalytic reduction of NO with CO over A-Cu-BTC and AO_x/CuO_y/C catalyst[J]. *Inorganic Chemistry Communications*, 2016, **72**: 78 - 82. DOI: 10. 1016/j. inoche. 2016. 08. 018.

[6] Xu W T, Zhou J C, Li H, et al. Microwave-assisted catalytic reduction of NO into N_2 by activated carbon supported Mn_2O_3 at low temperature under O_2 excess[J]. *Fuel Processing Technology*, 2014, **127**: 1 - 6. DOI: 10. 1016/j. fuproc. 2014. 06. 005.

[7] Wang Y L, Li X X, Zhan L, et al. Effect of SO_2 on activated carbon honeycomb supported CeO_2-MnO_x catalyst for NO removal at low temperature[J]. *Industrial & Engineering Chemistry Research*, 2015, **54**(8): 2274 - 2278. DOI: 10. 1021/ie504074h.

[8] Yao L, Liu Q C, Mossin S, et al. Promotional effects of nitrogen doping on catalytic performance over manganese-containing semi-coke catalysts for the NH_3-SCR at low temperatures[J]. *Journal of Hazardous Materials*, 2020, **387**: 121704. DOI: 10. 1016/j. jhazmat. 2019. 121704.

[9] Putluru S S R, Schill L, Jensen A D, et al. Mn/TiO_2 and Mn-Fe/TiO_2 catalysts synthesized by deposition precipitation: Promising for selective catalytic reduction of NO with NH_3 at low temperatures[J]. *Applied Catalysis B: Environmental*, 2015, **165**: 628 - 635. DOI: 10. 1016/j. apcatb. 2014. 10. 060.

[10] Liu Y J, Qu Y F, Guo J X, et al. Thermal regeneration of manganese supported on activated carbons treated by HNO_3 for desulfurization[J]. *Energy & Fuels*, 2015, **29**(3): 1931 - 1940. DOI: 10. 1021/ef502655k.

[11] Gu T, Gao F Y, Tang X L, et al. Fe-modified Ce-MnOx/ACFN catalysts for selective catalytic reduction of NO_x by NH_3 at low-middle temperature[J]. *Environmental Science and Pollution Research*, 2019, **26**(27): 27940 - 27952. DOI: 10. 1007/s11356-019-05976-4.

[12] Yang J, Ren S, Zhang T S, et al. Iron doped effects on active sites formation over activated carbon supported Mn-Ce oxide catalysts for low-temperature SCR of NO[J]. *Chemical Engineering Journal*, 2020, **379**: 122398. DOI: 10. 1016/j. cej. 2019. 122398.

[13] Zhang J, Sun J B, Ahmed Shifa T, et al. Hierarchical MnO_2/activated carbon cloth electrode prepared by synchronized electrochemical activation and oxidation for flexible asymmetric supercapacitors[J]. *Chemical Engineering Journal*, 2019, **372**: 1047 - 1055. DOI: 10. 1016/j. cej. 2019. 04. 202.

[14] Li Y, Xu Z Y, Wang D W, et al. Snowflake-like core-shell α-MnO_2@δ-MnO_2 for high performance asymmetric supercapacitor[J]. *Electrochimica Acta*, 2017, **251**: 344 - 354. DOI: 10. 1016/j. electacta. 2017. 08. 146.

[15] Pasel J, Käßner P, Montanari B, et al. Transition metal oxides supported on active carbons as low temperature

catalysts for the selective catalytic reduction (SCR) of NO with NH_3[J]. *Applied Catalysis B: Environmental*, 1998, **18**(3/4): 199-213. DOI:10.1016/S0926-3373(98)00033-2.
[16] Zeng S W, Zhao R R, Li A J, et al. MnO/Carbon fibers prepared by an electrospinning method and their properties used as anodes for lithium ion batteries[J]. *Applied Surface Science*, 2019, **463**: 211-216. DOI:10.1016/j.apsusc.2018.08.233.
[17] Kamran U, Heo Y J, Lee J W, et al. Chemically modified activated carbon decorated with MnO_2 nanocomposites for improving lithium adsorption and recovery from aqueous media[J]. *Journal of Alloys and Compounds*, 2019, **794**: 425-434. DOI:10.1016/j.jallcom.2019.04.211.
[18] Saputra E, Muhammad S, Sun H Q, et al. Manganese oxides at different oxidation states for heterogeneous activation of peroxymonosulfate for phenol degradation in aqueous solutions[J]. *Applied Catalysis B: Environmental*, 2013, **142/143**: 729-735. DOI:10.1016/j.apcatb.2013.06.004.
[19] Shan J, Wang J J, Zhao Y, et al. Nitrogen-doped porous carbon/Mn_3O_4 composites as anode materials for lithium-ion batteries[J]. *Solid State Sciences*, 2019, **92**: 89-95. DOI:10.1016/j.solidstatesciences.2019.03.001.
[20] Lin Y T, Li Y R, Xu Z C, et al. Transformation of functional groups in the reduction of NO with NH_3 over nitrogen-enriched activated carbons[J]. *Fuel*, 2018, **223**: 312-323. DOI:10.1016/j.fuel.2018.01.092.
[21] Liu Z, Wang Z J, Qing S J, et al. Improving methane selectivity of photo-induced CO_2 reduction on carbon dots through modification of nitrogen-containing groups and graphitization[J]. *Applied Catalysis B: Environmental*, 2018, **232**: 86-92. DOI:10.1016/j.apcatb.2018.03.045.
[22] Yu J, So J. Synthesis and characterization of nitrogen-containing hydrothermal carbon with ordered mesostructure[J]. *Chemical Physics Letters*, 2019, **716**: 237-246. DOI:10.1016/j.cplett.2018.12.014.
[23] Bian Y, Bian Z Y, Zhang J X, et al. Adsorption of cadmium ions from aqueous solutions by activated carbon with oxygen-containing functional groups[J]. *Chinese Journal of Chemical Engineering*, 2015, **23**(10): 1705-1711. DOI:10.1016/j.cjche.2015.08.031.
[24] Deng L L, Lu B Q, Li J L, et al. Effect of pore structure and oxygen-containing groups on adsorption ofdibenzothiophene over activated carbon[J]. *Fuel*, 2017, **200**: 54-61. DOI:10.1016/j.fuel.2017.03.018.
[25] Fan Q Y, Sun J X, Chu L, et al. Effects ofchemical oxidation on surface oxygen-containing functional groups and adsorption behavior of biochar[J]. *Chemosphere*, 2018, **207**: 33-40. DOI:10.1016/j.chemosphere.2018.05.044.
[26] Ambrico Y, Castro M A, Lee J, et al. Adsorption of creatinine on active carbons with nitric acid hydrothermal modification[J]. *Journal of the Taiwan Institute of Chemical Engineers*, 2016, **66**: 347-356. DOI:10.1016/j.jtice.2016.06.008.
[27] Lakshmi S D, Avti P K, Hegde G. Activated carbon nanoparticles from biowaste as new generation antimicrobial agents: A review[J]. *Nano-Structures & Nano-Objects*, 2018, **16**: 306-321. DOI:10.1016/j.nanoso.2018.08.001.
[28] Thirupathi B, Smirniotis P G. Nickel-doped Mn/TiO_2 as an efficient catalyst for the low-temperature SCR of NO with NH_3: Catalytic evaluation and characterizations[J]. *Journal of Catalysis*, 2012, **288**: 74-83. DOI:10.1016/j.jcat.2012.01.003.

$Mn(NO_3)_2$ 对椰壳活性炭改性机理

黄帮福 施 哲 蔡 鸣 于安和

(昆明理工大学冶金与能源工程学院, 昆明 650093)
(昆明理工大学云南省高校复杂铁资源清洁冶金重点实验室, 昆明 650093)

摘要: 为探明 HNO_3 和 $Mn(NO_3)_2$ 对活性炭改性机理,采用 HNO_3、$Mn(NO_3)_2$ 先后对椰壳活性炭进行活化和改性,对改性前后炭材料孔结构和表面化学性质进行 SEM、BET、XRD、FTIR 和 XPS 表征. 硝酸改性后活性炭表面微孔变形、相邻孔合并,Mn/AC-1 表面负载物总体呈块体和网状纤维结构,MnO_x 呈细小碎块晶体散落在 Mn/AC-2 表面,Mn/AC-3 表面负载物以大量纱状超薄纳米片交错填充在孔道中. HNO_3 活化可起到扩孔作用但会降低 AC 比表面积;Mn 负载可构造出新孔隙结构,提高总比表面积、微孔比表面和微孔孔容;5% 负载量和 500 ℃煅烧温度可制得孔结构参数较优的 Mn/AC-2 催化剂. HNO_3 改性可明显降低活性炭灰分,Mn/AC-1 表面负载物主要为 Mn_3O_4 和少量 Mn_2O_3,Mn/AC-2 负载物主要为 Mn_3O_4 和一定数量的 MnO,Mn/AC-3 表面负载物几乎全部为 Mn_3O_4. HNO_3 活化和 Mn 负载改性均对官能团类型没有影响. 相同负载量下提高煅烧温度则会降低 O—H 键和 N—H 键数量同时增加 C═C 键和 C—O 键数量;相同煅烧温度下,负载量越高则 O—H 键和 N—H 键越多. 高负载量有利于 Mn^{4+} 物种增加,提高煅烧温度可增加 Mn^{3+} 物种. 研究成果可为优化 Mn/AC 催化剂制备和提高炭基催化剂理化性能提供借鉴.

关键词: HNO_3; $Mn(NO_3)_2$; 椰壳活性炭; 理化性质; 改性机理
中图分类号: TQ520